Al-Khwarizmi Engineering Journal, Vol.4 , No.1 , pp 27-47 (2008)

Al-khwarizmi
Engineering
Journal

The Effects of Vortex Generator Types on Heat Transfer and Flow Structure in a Rectangular Duct Flows

Dr. Waheed S. Mohammed
Asst. Prof. Mech. Eng. Dep.
University of Technology
Baghdad – IRAQ

Dr. Sabah Tarik Ahmed
Asst. Prof. Mech. Eng. Dep.
University of Technology
Baghdad – IRAQ

Laith J.H.
Asst. Lect. Mech. Eng. Dep.
University of Technology
Baghdad – IRAQ

(Received 25 July 2006; accepted 2 January 2008)

Abstract:

In this numerical study a detailed evaluation of the heat transfer characteristics and flow structure in a laminar and turbulent flow through a rectangular channel containing built-in of different type vortex generator has been a accomplished in a range of Reynolds number between 500 and 100,000.A modified version of ESCEAT code has been used to solve Navier-Stokes and energy equations. The purpose of this paper is to present numerical comparisons in terms of temperature, Nusselt number and flow patterns on several configurations of longitudinal vortex generator including new five cases. The structures of heat and flow were studied, using iso-contours of velocity components, vortices, temperature and Nusselt number. This study shows that the predicted structures of fluid flow, temperature fields and Nusselt number variation are strongly affected by the presence of the turbulators. Staggered arrangement gains high Nusselt number, also the lower and upper arrangements have higher Nusselt number than plane duct. High Reynolds number (higher air inlet velocity) will enhance the Nusselt number. Increase in ribs height will enhance the heat transfer as it works as surface area and turbulator at the same time.

Keywords: CFD Turbulators, Heat Transfer and Fluid Flow, Rectangular Duct.

Introduction:

Boundary Layer control is any mechanism or process through which the boundary Layer is caused to behave differently than it normally would, were the flow developing naturally along a smooth straight surface. Examples include reduction / delay or enhancement / triggering of transition, separation, skin friction, or pressure drop, heat transfer, lift, and acoustics. A relatively popular device used in flow control schemes is the vortex generator, VG. These are typically small airfoils that extent from the surface into the flow and produce stream wise vorticity within the boundary layer. Vortex generator and micro-VGs are passive control devices, which work well under a narrow range of flow conditions as a result of their inability to be actively varied in response to changes in the flow field. The passive VGs have been used with success, however, they cannot be removed from the flow when unneeded which result in significant parasitic drag. Others control systems have used vibrating surfaces, such as small flaps or ribbons, to generate a wall-normal component of velocity within the boundary layer [1].

Most previous studies were related to a single circular cylinder or rectangular bluff body immersed in free streams, while other studies are pertinent to flow passing through bluff bodies in confined ducts.

For confined turbulent flows past bodies, which usually occur in practice, stochastic three-dimensional turbulent fluctuations are superimposed on the periodic vortex-shedding motion in the wake region. The simulation of large coherent structures in the turbulent wake is difficult because of the widespread spectrum of scales. A resolution of these motions in a direct simulation is not feasible at present. Hence, there is still a need for economic calculation methods based on the use of a turbulence model for simulating the influence of the stochastic fluctuations on the periodic vortex-shedding motion [2].

Heat transfer enhancement techniques are found in many of today's processes. Devices such as inclined baffles, rib tabulators, jet impingement, etc. are all used in order to augment the thermal transfer of a process.

In applications such as air-cooled solar collectors laser curtain seals electronic cooling, gas-liquid heat exchangers, etc., gases are used instead of liquids as the heat transfer medium. Gases inherently have lower heat transfer rates than liquids; therefore heat transfer enhancement techniques that maximize heat transfer are of particular interest. Some of the most common heat transfer augmentation techniques are (1) periodic placement of ribs on the heat transfer surface to create boundary layer disturbances; (2) impingement techniques, where high-velocity gas jest are directed at the surface in order to cool it ; (3) internal flow swirls or tape twisters used to create high-levels of turbulence , which , in turn , augment heat transfer ; (4) high free – stream turbulence created by high-velocity jets , situated to inject air flow normal to the mainstream cross flow [3]. In electronic devices cooling, for example, and along with the progress of the semiconductor technology, the recent trend in developing electronic devices is toward increased miniaturization of components and compact packaging which result in more heat being generated by the electronic devices and the junction temperature of the electronic devices being higher. The failure rate of the electronic device been statistically corrected to be proportional to the exponential of the electronic device junction temperature. Thus the thermal problem has become important for the reliability and performance of new electronic devices and how to enhance heat transfer becomes critical. Vortices may naturally induce a flow toward the heat transfer surface. This behavior could augment transverse fluid mixing and reduce the thermal boundary layer thickness. Thus the local heat transfer could be enhanced in the neighborhood of the vortices [4].

Experimental and numerical studies on the fluid flow and heat transfer in channels with wing-type VGs were carried out by several researchers [5-8]. In spite of the different Reynolds numbers and wing's dimensions and arrangements, the researchers results show that the VGs can generate transfer, longitudinal and horseshoe vortices. These vortices have influences on the velocity and temperature fields and strongly disturb the flow structure. These factors are reasons for heat transfer enhancement by VGs.

The effect of rib orientation on local heat transfer distributions and pressure drop in a channel with multi-ribbed walls for a range of Reynolds number have been investigated by other researchers [9 & 11]. They also studied the effect of ribs configurations and geometries on the flow and temperature fields. Taking both thermal and flow aspects into consideration simultaneously, Nusselt number and coefficient of pressure drop increase hand in hand with increasing ratio of promoter height to channel spacing. This tendency is consistent with the increased levels of flow disturbance or turbulence mixing, promoted by the protruding ribs and the installed turbulence promoter. In addition, the permeable ribbed geometry provides a higher thermal performance than the solid-type ribbed, and the best thermal performance occurs.

The initiation and subsequent development of the vortex- shedding phenomenon was investigated by Davis &Moore [12] .The properties of these vortices were found to be strongly dependent on Reynolds number. The numerical solution was for two-dimensional time-dependent flow for Reynolds-number from 100-2800.An experimental investigation of a longitudinal vortex embedded in a turbulent boundary layer was made by Eibeck & Eaton [13] to increase the physical understanding of the heat transfer effect of a longitudinal vortex. They found that longitudinal vortices usually maintain their coherence over a long, stream wise distance, meaning that the heat transfer effects behind an effective VG are likely to be very persistent.

From this previous work review, it found that the most researches were experimental and the numerical studies using CFD for three-dimensional laminar and turbulent flows for multi-type VGs were few, thus, the main objective of the present study is to investigate the effect of different pattern flows using several obstacles. The ducts configurations and the several types VGs are presented in figure (1) and table (1).

Governing Equations and Numerical Details

The governing three-dimensional elliptic (PDES) are based on the conservation of mass, momentum and thermal energy. The governing equations of turbulent flow field based on time averaged are as follows [14&15]:

(i)Continuity equation:-

$$\frac{\partial U}{\partial x}+\frac{\partial V}{\partial y}+\frac{\partial W}{\partial z}=0 \quad \ldots\ldots\ldots\ldots\ldots\ldots\ldots\ldots \quad (1)$$

(ii) Momentum equation:-

X-momentum equation:

$$\frac{\partial (U^2)}{\partial x}+\frac{\partial (UV)}{\partial y}+\frac{\partial (UW)}{\partial z}=-\frac{1}{\rho}\frac{\partial P}{\partial x}+\frac{\partial}{\partial x}\left(\nu_{eff}\frac{\partial U}{\partial x}\right)+\frac{\partial}{\partial y}\left(\nu_{eff}\frac{\partial U}{\partial y}\right)+\frac{\partial}{\partial z}\left(\nu_{eff}\frac{\partial U}{\partial z}\right)+\frac{\partial}{\partial x}\left(\nu_{eff}\frac{\partial U}{\partial x}\right)+\frac{\partial}{\partial y}\left(\nu_{eff}\frac{\partial V}{\partial x}\right)+\frac{\partial}{\partial z}\left(\nu_{eff}\frac{\partial W}{\partial x}\right) \quad \ldots\ldots\ldots\ldots \quad (2)$$

Y-momentum equation:

$$\frac{\partial (UV)}{\partial x}+\frac{\partial (V^2)}{\partial y}+\frac{\partial (VW)}{\partial z}=-\frac{1}{\rho}\frac{\partial P}{\partial y}+\frac{\partial}{\partial x}\left(\nu_{eff}\frac{\partial V}{\partial x}\right)+\frac{\partial}{\partial y}\left(\nu_{eff}\frac{\partial V}{\partial y}\right)+\frac{\partial}{\partial z}\left(\nu_{eff}\frac{\partial V}{\partial z}\right)+\frac{\partial}{\partial x}\left(\nu_{eff}\frac{\partial U}{\partial y}\right)+\frac{\partial}{\partial y}\left(\nu_{eff}\frac{\partial V}{\partial y}\right)+\frac{\partial}{\partial z}\left(\nu_{eff}\frac{\partial W}{\partial y}\right) \quad \ldots\ldots\ldots\ldots \quad (3)$$

Z-momentum equation:

$$\frac{\partial (UW)}{\partial x}+\frac{\partial (VW)}{\partial y}+\frac{\partial (W^2)}{\partial z}=-\frac{1}{\rho}\frac{\partial P}{\partial z}+\frac{\partial}{\partial x}\left(\nu_{eff}\frac{\partial W}{\partial x}\right)+\frac{\partial}{\partial y}\left(\nu_{eff}\frac{\partial W}{\partial y}\right)+\frac{\partial}{\partial z}\left(\nu_{eff}\frac{\partial W}{\partial z}\right)+\frac{\partial}{\partial x}\left(\nu_{eff}\frac{\partial U}{\partial z}\right)+\frac{\partial}{\partial y}\left(\nu_{eff}\frac{\partial V}{\partial z}\right)+\frac{\partial}{\partial z}\left(\nu_{eff}\frac{\partial W}{\partial z}\right) \quad \ldots\ldots\ldots\ldots \quad (4)$$

(iii) Energy equation:

$$\frac{\partial\, UT}{\partial x}+\frac{\partial V\,T}{\partial y}+\frac{\partial W\,T}{\partial z}=\frac{\partial}{\partial x}\left(\Gamma_{eff}\frac{\partial T}{\partial x}\right)+\frac{\partial}{\partial y}\left(\Gamma_{eff}\frac{\partial T}{\partial y}\right)+\frac{\partial}{\partial z}\left(\Gamma_{eff}\frac{\partial T}{\partial z}\right) \quad \ldots\ldots\ldots . \quad (5)$$

Where: $\upsilon_{eff}=\upsilon_{l}+\upsilon_{t}$ & $\Gamma_{eff}=\Gamma_{l}+\Gamma_{t}$ and

$$\Gamma_l=\frac{\nu_l}{Pr_l};\ \Gamma_t=\frac{\nu_t}{Pr_t};\ Pr=\frac{\mu\cdot Cp}{K}$$

The standard k-ε turbulent model:

The standard k-ε model uses the following transport equations for k and ε :

$$\frac{\partial}{\partial x}(kU)+\frac{\partial}{\partial y}(kV)+\frac{\partial}{\partial z}(kW)=\frac{\partial}{\partial x}\left(\frac{v_t}{Pr_k}*\frac{\partial k}{\partial x}\right)+\frac{\partial}{\partial y}\left(\frac{v_t}{Pr_k}*\frac{\partial k}{\partial y}\right)+\frac{\partial}{\partial z}\left(\frac{v_t}{Pr_k}\frac{\partial k}{\partial z}\right)+G-\varepsilon \quad \ldots\ldots \quad (6)$$

$$\frac{\partial}{\partial x}(\varepsilon U)+\frac{\partial}{\partial y}(\varepsilon V)+\frac{\partial}{\partial z}(\varepsilon W)=\frac{\partial}{\partial x}\left(\frac{v_t}{Pr_\varepsilon}*\frac{\partial \varepsilon}{\partial x}\right)+\frac{\partial}{\partial y}\left(\frac{v_t}{Pr_\varepsilon}*\frac{\partial \varepsilon}{\partial y}\right)+\frac{\partial}{\partial z}\left(\frac{v_t}{Pr_\varepsilon}*\frac{\partial \varepsilon}{\partial z}\right)+C_{1\varepsilon}\cdot\frac{\varepsilon}{k}-G-C_{2\varepsilon}\cdot\frac{\varepsilon^2}{k} \quad \ldots\ldots\ldots\ldots \quad (7)$$

Where:

$$G=\nu_t\Big[2\left(\frac{\partial U}{\partial x}\right)^2+2\left(\frac{\partial V}{\partial y}\right)^2+2\left(\frac{\partial W}{\partial z}\right)^2+\left(\frac{\partial U}{\partial y}+\frac{\partial V}{\partial x}\right)^2+\left(\frac{\partial U}{\partial z}+\frac{\partial W}{\partial x}\right)^2+\left(\frac{\partial U}{\partial z}+\frac{\partial W}{\partial y}\right)^2 \quad \ldots\ldots\ldots\ldots \quad (8)$$

Wall function employed

The implementation of the wall boundary conditions starts with evaluation of dimensionless quantity. In turbulent flow:

$$y^+=C_\mu^{0.25}\cdot\rho\cdot k_P^{0.5}\cdot\frac{y_P}{\mu} \quad \ldots\ldots\ldots \quad (9)$$

Where y_P is the distance of near wall node (P) to the solid surface. A near wall flow is assumed to be laminar if $y^+\le 11.5$ and turbulent if $y^+>11.5$. Constant shear stress (τ_{wall}) will be assumed through the wall region:

$\tau_{wall}=\mu\cdot\frac{U_P}{y_P}$ Where U_P is the velocity at the grid node.

The wall force is represented in the discredited momentum equations as follows:

$$F_s=-\tau_{wall}\cdot A_{cell} \quad \ldots\ldots\ldots\ \ldots\ldots\ldots\ \ldots \quad (10)$$

The wall force is introduced into the discredited equation as source term , so

$$S_p = -\frac{\mu}{y_p}\cdot A_{cell} \qquad \text{For} \quad y^+ \le 11.5 \quad ....(11)$$

$$S_p = \frac{-\rho\cdot C_\mu^{1/4}\cdot k_p^{1/2}\cdot \kappa}{Ln\left(Ey^+\right)} \qquad \text{For} \quad y^+ > 11.5 \quad ......(12)$$

Where $\kappa = 0.41$ and $E = 8.4$

The source terms for the turbulent flow in the discredited k-equation are represented as:

$$\left.\begin{aligned} S_p &= -\rho\cdot C_\mu^{3/4}\cdot k_p^{1/2}\cdot Ln\left(\frac{Ey^+}{\kappa\, y_p}\right)\cdot\Delta V \\ S_u &= \frac{-\tau_w\cdot U_p}{y_p}\cdot\Delta V \end{aligned}\right\} ....(13)$$

Where ΔV is the wall control volume. The discredited ε-equation is fixed to the value:

$$\varepsilon_p = \frac{C_\mu^{3/4}\cdot k_p^{3/2}}{\left(\kappa\cdot y_p\right)} \qquad .... \; .... \; .... \quad (14)$$

In the discredited ε-equation the near wall node is fixed to the given value in Eq.(14) by means of setting the source terms S_p and S_u as follows:

$$\left.\begin{aligned} S_p &= -10^{30} \\ S_u &= \frac{C_\mu^{3/4}\cdot k_p^{3/2}}{\kappa\cdot y_p}\times 10^{30} \end{aligned}\right\} .... \; .... \; .(15)$$

There are several differencing schemes available for use in deriving the FDES from their PDES, however, power-law scheme is used in this paper.

The coefficients in this scheme read:

$$\left.\begin{aligned} a_E &= D_e < 0,(1-0.1\frac{|F_e|}{D_e})^5 > + < 0,-F_e > \\ a_W &= D_w < 0,(1-0.1\frac{|F_e|}{D_w})^5 > + < 0,+F_w > \end{aligned}\right\} ....(16)$$

Which means that;

$$\left.\begin{aligned} a_E &= -F_e & &\text{if} \quad Pe < -10 \quad , \\ a_E &= D_e(1-0.1\frac{|F_e|}{D_e})^5 - F_e & &\text{if} \quad -10 \le Pe < 0 \quad , \\ a_E &= D_e(1-0.1\frac{|F_e|}{D_e})^5 & &\text{if} \quad 0 \le Pe \le 10 \quad ,\text{and} \\ a_E &= 0.0 & &\text{if} \quad Pe > 10 \end{aligned}\right\} ....(17)$$

Nusselt number

i) Laminar case:

The local Nusselt number on the duct walls and on the obstacles surfaces is defined by:

$$Nu = \frac{\partial T^+}{\partial n^+} = \frac{(T_n - T_{wall})/T_{in}}{\Delta n / N} \qquad ....\;...... \quad (18)$$

The average Nusselt number was calculated by numerical integration over the length of the lines of the surface and then over the length of the channel using trapezoidal method.

ii) Turbulent case:

The local Nusselt number:

$$Nu = St\cdot\frac{hd\cdot Pr_t}{\mu}\cdot\left|\frac{(T_n - T_{wall})\cdot\rho\cdot w_n}{(Tb - T_{wall})}\right| \qquad .... \quad (19)$$

Where:

$$St = \frac{|\tau_w|/\rho\cdot U_P^{\,2}}{Pr_t\cdot(1+P_J\sqrt{\frac{|\tau_w|}{\rho\cdot U_P^{\,2}}})} \quad , \quad P_J = 9.0\cdot(\frac{Pr_l}{Pr_t}-1)\cdot(\frac{Pr_t}{Pr_l})^{1/4}$$

And for more details about (U_P) and (Tb) see Waheed [15]. Also the average Nusselt number was calculated as described in the laminar case.

The Applied Conditions

A. Initial $u = v = 0$, $w = w_{in}$, $k = k_{in} = 0.00135 * (w_{in})^2$, $\varepsilon = \varepsilon_{in} = 0.09 * (k_{in})^{1.5} / (0.03 * hd)$, $T = T_{ref}$

B. At inlet $u = v = 0$, $w = w_{in}$, $k = k_{in}$, $\varepsilon = \varepsilon_{in}$, $\mu = \mu_{ref}$, $T = T_{in}$

C. At walls and VGs surfaces $u = v = w = k = \varepsilon = 0$, $\mu = \mu_{ref}$, $T = T_{wall}$

D. At exit all variables equal to the same variables just before one plane.

A finite volume technique with staggered grids combined with the SIMPLE algorithm is used to solve Navier-Stokes and energy equations, Patanker [16].The VGs are represented by making the velocities (u, v, and w) are equal to zero at the baffle location grids, and the temperatures are equal to the temperature of the wall that the VGs are placed. For solving the finite difference equations, the calculation domain is divided into a number of control volumes. Each control volume is associated with particular dependent variable. In the method to be described, the aim is to calculate the main dependent variables at a number of chosen points called the grid points. The governing differential equations are discredited reduced to algebraic equations by constructing a control volume surrounding each grid point. There are several possible ways in which the control volumes are chosen. The most obvious way of constructing the control volumes in this study is to place their faces midway between neighboring grid points, see the Distribution bellow.

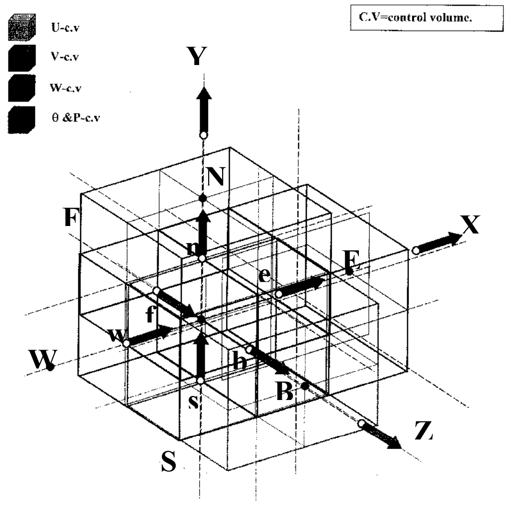

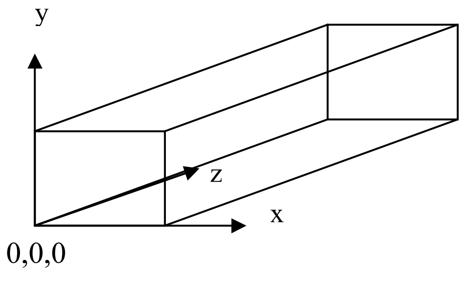

Results and Discussion

Using the previously described numerical method, computations have been carried out for flow and heat transfer. The parameters involved are VG types, Reynolds number, duct and VGs configurations and dimensions, will be discussed below, see table.

In order to justify the present computations, comparisons have been made with two sets of numerical predictions and experimental data from other sources.

Figure (2) shows comparison of an experimental data of Eibeck et al.[13], for laminar flow in a channel with built-in winglet type VG (case H). The results agree well with the experiment.

Figure (3) shows another comparison of the computational result of Sabah [17], with the present result for laminar flow in a smooth duct (1*1*2) m^3. Again both calculations display good agreement.

On the whole, it appears that the present procedure has demonstrated its ability to successfully simulate the development of the complex turbulent flow and other complicated flows using several VG configurations as shown in figure (1). One of these is case (A), it is presented in figure (4) which shows a 4-finned duct, the first pair at bottom wall at (z = 0.231 m) and the second pair at top wall at (z = 0.502 m). The obtained velocities, vectors, temperatures contours and Nusselt number are presented in this figure. Figure (4-a to d) are for laminar case where $T_{in}=20C^o$ and $T_{wall}=50C^o$ and figure (4-e&f) are for turbulent case where $T_{in}=10C^o$ and $T_{wall}=40C^o$.

Figure (4-a) presents the streamwise mean velocity vector fields around the fins at (x = 0.016 m). The approaching flow below the VG height is retarded and turned upward near VG's front edge to flow over the VG. It is interesting to note that there is no corner vortex formed in the front of the VGs. Comparison of the span wise-average Nusselt number distributions between upper and lower walls of the duct is tackled in figure (4-b). There is a peak on each of the curves of Nusselt number in front of VGs. After this peak and after the vortex generators the level of Nusselt number along the duct decreases and reaches to an approximately constant level. The local Nusselt number for the upper wall is shown in figure (4-c). The peaks are appearing clearly. Figure (4-d) represents the temperature contours at cross section (z = 0.502 m). It shows how the fins affected the thermal boundary layer. For turbulent flow, figure (4-e&f) shows the temperature contours at (z-y) plane and average Nusselt number for the four walls of the duct respectively. Fig. (4-e) shows the temperature variation along the duct at (x = 0.032 m). In fig. (4-f) the Nusselt number shows larger amplitude of the variation for the upper and lowers finned walls than the right and left walls.

Airflow in the duct and Nu variation on rib surfaces in a vertical ribbed duct (case B) are shown in figure (5). The rib location is at (x = 0.048 m & z = 0.382 m) and T_{in}=7 C^o while the wall or rib surface temperature is T_{wall}=27 C^o. Figure (5-a) gave the vectors of flow in three-dimensions at (z = 0.016, 0.133, 0.273, 0.413, 0.553 m), it shows the velocity distribution and how the rib affected the flow. While figure (5-b) gave the average Nu variation on rib surfaces, it is appearing that the front surface have the larger Nu than the rear face.

The effects of horizontal fin (case C) on the temperature and Nu for laminar flow are shown in fig. (6), the fin at (z = 0.382 m & y = 0.04 m) and (T_{in}=7 C^o & T_{wall}=27 C^o). Fig. (6-a) shows the temperature contours at (z = 0.382 m), it shows how the fin makes an additional heated object to add new thermal boundary layer. The average Nu along the faces of the fin can be seen in fig. (6-b) which shows the low Nu near the ends of the fin because the effect of the thermal boundary layer.

Fig. (7) highlighted the effects of case D on the flow, temperature and Nu for laminar and turbulent flows, the horizontal rib at (z = 0.484 m & y = 0.09 m) and the vertical one at (z = 1.054 m & x = 0.18 m) while (T_{in}=16 C^o & T_{wall}=40 C^o) for laminar flow and (T_{in}=10 C^o & T_{wall}=40 C^o) for turbulent flow. Fig. (7-a) represents the temperature contours for laminar flow at (z = 0.057, 0.256, 0.541, 0.826, 1.111, 1.395, and 1.68 m), it is clear that the ribs make a circular contours of the temperatures. While fig. (7-b) shows the isotherms at (y = 0.09 m), it can be seen that the ribs increase the mixing between the cold flow and the hot surfaces. The variation of Nu has been represented in fig. (7-c to e) for laminar case. Fig. (7-c) shows the variation of average Nu at the horizontal rib surfaces, and fig. (7-d) at the vertical rib surfaces, it show that large Nu occurs in the middle of the ribs. Fig. (7-e) highlighted the local Nu at the left surface of the vertical rib. The turbulent flow are tackled in fig. (7-f&g), where fig. (7-f) shows the velocity (u-v) vectors at the end of the duct, the vortices are very clear in this figure, while fig. (7-g) shows the velocity (w/w_{in}) vectors at (x-z) plane (y = 0.09 m), it is appear how the ribs change the velocity distribution in the end of the duct.

Fig. (8) presents case E for laminar flow, where fig. (8-a) gave the (u/w_{in} -component) velocity at (z = 0.382 m) and shows the symmetric contours. Fig. (8-b) gave the (v/w_{in} -component) velocity at the same position and shows the symmetric values of the velocity at the beginning of the duct.

For oblique VG (case F), fig. (9) depicts temperatures, velocities, and Nusselt numbers for laminar and turbulent flows. The vortex structure is weakened or even broken after its retardation by the divider wall. As a result, Nu decreases as described in fig. (9-a&b) for laminar flow where (T_{in}=20 C^o & T_{wall}=50 C^o) and fig. (9-b) for bottom wall. For turbulent flow pattern, fig. (9-c) depicts the (v-component) velocity contours along the duct at (z = 0.027, 0.095, 0.204, 0.339, 0.475, 0.611, and 0.746 m). The velocity contours (w/w_{in}) at station (z = 0.393 m) are depicted in fig. (9-d). There are strong interactions between the longitudinal vortices and the boundary layer on the walls of the duct, especially the lower wall. These interactions affect the structure of the velocity or the thermal boundary layer by thinning it in the downwash region on the lower wall while the opposite trend occurs on the upper wall, see (v-component) velocity contours (fig. (9-c)) and cross flow velocity contours (fig. (9-d)) and temperature contours along the duct (fig. (9-e)) at (x = 0.16 m) where (T_{in}=10 C^o & T_{wall}=40 C^o). The average Nu variations along the duct for the four walls are tackled in fig. (9-f) for turbulent flow. The highest Nu compared with the laminar case (fig. (9-a)) is due to the effects of the additional variables of shear stress and high velocities.

The effect of broken rib (case G) on velocities, Nusselt, Stanton numbers are presented in fig. (10). The first rib is placed at (z = 0.312 m) and the other at (z = 0.583 m). For laminar flows where (T_{in}=20 C^o &

T_{wall}=50 C^o), fig. (10-a) shows that when the VGs are exposed to the main flow, due to pressure difference between two sides of VG, flow separation occurs and longitudinal vortices are generated. Fig. (10-b) represents local Nu for left wall, it shows how the Nu increases because of the increase of heat transfer area and temperature difference and the influence of the vortices. Fig. (10-c) shows span wise local Nu, Nu(z), in the stream wise direction. The Nu(z) fluctuates in the regions where the VGs exist. On the other hand, the variation of Nu(z) are approximately similar in the upstream of VGs. And for turbulent flows where (T_{in}=10 C^o & T_{wall}=40 C^o), fig. (10-d) represents velocity (w) vectors in (x-z) plane, it can be seen that the presence of ribs causes the flow to bend and impinge significantly on the right and left walls and on the upstream surface of ribs. The average Nu described in fig. (10-e), it shows a small increase in the Nu in the beginning of the duct and an increase of Nn(z) in VGs region. The local Stanton number presented in fig. (10-f), it is appear that the Stanton number increases in front of the ribs and then decreases behind the ribs and then increases again and decreases downstream.

Figure (11) describes the simulation of laminar and turbulent flow for delta winglet and winglet pair (case H & case I). Fig. (11-a) describes the local Nu for case H for laminar flow where (T_{in}=16 C^o & T_{wall}=40 C^o), it shows that the winglet divide the duct into two similar parts and then increase Nu very little. For turbulent flow where (T_{in}=10 C^o &T_{wall}=40 C^o), fig. (11-b) describes the secondary velocity vectors (u-v components) for case I. As the vortex developed, the secondary velocities decreased and the core radius increased.

Case J is presented in figure (12), the laminar flow are tackled in fig. (12-a to d) where (T_{in}=7 C^o & T_{wall}=27 C^o), while the turbulent flow are tackled in fig. (12-e to g) where (T_{in}=10 C^o & T_{wall}=40 C^o). A small recirculation zone is found behind the lower heated obstacles as shown in fig. (12-a). Weak clockwise vortices are formed within the grooves, which is similar to the cavity flow. These recirculation zones and vortices are impediments to the heat transfer from the heated obstacles. The temperature contours are shown in fig. (12-b) at (z = 0.142 m), which described the isotherms distribution across the duct as a hot rib and walls and cold core. Fig. (12-c) shows the isotherms at (z = 0.144 m), it is clear that the upper rib increases the mixing layer and then enhances heat transfer. The variations of average Nu along the ribs face are indicated in fig. (12-d), which indicates that the values of Nu distribution surrounding the back face of the upper rib are higher than for other ribs. This indicates that a smaller recirculating vortex exists behind the upper rib compared to subsequent ribs. Fig. (12-e) indicates the stereamwise mean velocity (w) contours; it shows the small vortices that formatted behind the solid bottom ribs. Fig. (12-f) illustrates the average Nu for the four-sided duct. The results show that the average Nu on the ribbed sidewall has large fluctuations decreases slowly with distance, due to flow separation from ribs and decreases after flow reattaching on the surface and then increase again before flow hits next rib. The local Stanton numbers for the bottom wall are illustrated in fig. (12-g). Several features are immediately appearing. The first vortex causes a peak augmentation of the local St, and then the local heat transfer coefficient. The span wise variations in the St can be directly related to the mean velocity field. The minimum in the St curve is associated with the up wash region, where warm, low-momentum fluid from the near-wall zone is swept up ward to thicken the boundary layer.

Finally, fig. (13) shows the effect of case K on velocity, temperature, Nu and St numbers for laminar flow (fig. (13-a to d)) and for turbulent flow (fig. (13-e to g)) where (T_{in}=10 C^o & T_{wall}=40 C^o). Fig. (13-a) indicates the temperature contours at (z = 0.531 m), the influence of the vortex pair is very clear. And the average Nu has been presented in fig. (13-b) for the four-sided wall. It is clear that the roughened walls have a large value than the smooth walls. It can bee seen from this figure that the average Nu for right and left walls starts out high and then gradually tapers off. This is to be expected as the thermal boundary layer develops within the duct. And for top finned wall, it can be seen that the fins result in higher average Nu, it is also observed that the addition of the fins produces an oscillating shape in the curve of the Nu along the duct.

Also for bottom-baffled wall, a higher Nu is achieved. Here, the baffle increases the local airflow velocity at the heated surface by reducing the cross-sectional area of the duct. The local Nu for top wall with 4-fins and for bottom wall with wing-type VG are presented in fig. (13-c & d) respectively. High Nu can be attributed to the fact that the turbulators are causing flow separation and reattachment, as well as interrupting the boundary layer, causing high turbulence local to the heated surface. The periodicity in fig. (13-b & c) can be attributed to the periodic placement of the fins and the fact that the flow separation is occurring before and after the fins. These points of separation result in local “hotspots”, which translate into a reduction in the Nusselt numbers. Fig. (13-e) at ($z = 1.68$ m) shows that for delta wing in a duct flow the divergence of the vortex axes prevails but the cross-section becomes strongly elliptic. The symmetry planes set limits to the possible divergence of the vortices, and the walls set limits to their vertical movement. Fig. (13-f) illustrate the St for bottom wall with wing-type VG, it shows large fluctuations decreases with distance. Fig. (13-g) shows the average Nu for the four walls, the upper and lower roughened walls have a larger value than the right and left smooth walls.

Conclusions

The following are been concluding from the present work:

1. Longitudinal vortices of moderate size and strength have been found to cause a significant perturbation in the heat transfer behavior of an otherwise three-dimensional boundary layer. Local St increases and decreases, resulting in a net increase in the span wise-averaged heat transfer coefficient or Nu.
2. The use of a turbulence promoter can effectively improve the heat transfer characteristics and avoid the occurrence of hotspots in the high-temperature regime. In addition, it enhances not only the heat transfer performance of its downstream ribs, but also that of its upstream ribs.
3. When the side-wall confinement is appropriately utilized, most of the up wash sides of the longitudinal vortex pairs induced by the VGs arranged in a proper pitch can be truncated resulting in a large area of the vortex-generator mounted wall exposed to the downwash sides of the longitudinal vortex pairs and, in turn, high heat transfer augmentation.
4. The VGs are punched out of the fin and they generate swirling motion in the flows in the duct formed by the fin and thereby increase the heat transfer.
5. With the exception of the configurations, the addition of ribs always improved the average Nu number.
6. Combining ribs with baffles yielded an increase in average Nu. Therefore, a situation where rate of heat transfer is critical to the performance of a device combining ribs with baffle is a viable solution.

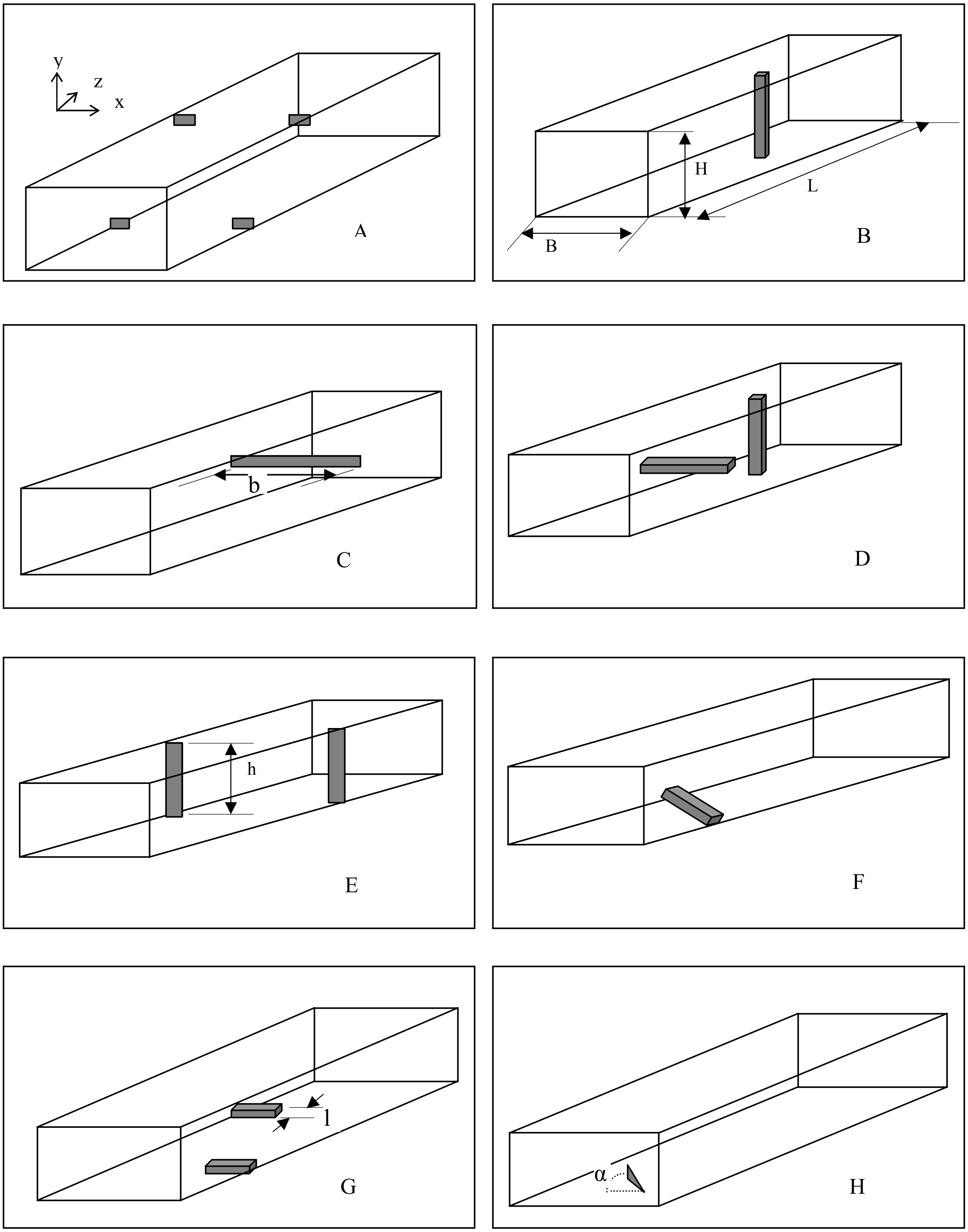

Fig. (1) Types of Vortex Generators used (the figures not to scale): A) Fins, B) Vertical rib ,C) Horizontal fin, and D) Horizontal & vertical rib,E) Vertical fins, and F) Oblique rib ,G) Staggered ribs, H) Delta-winglet.

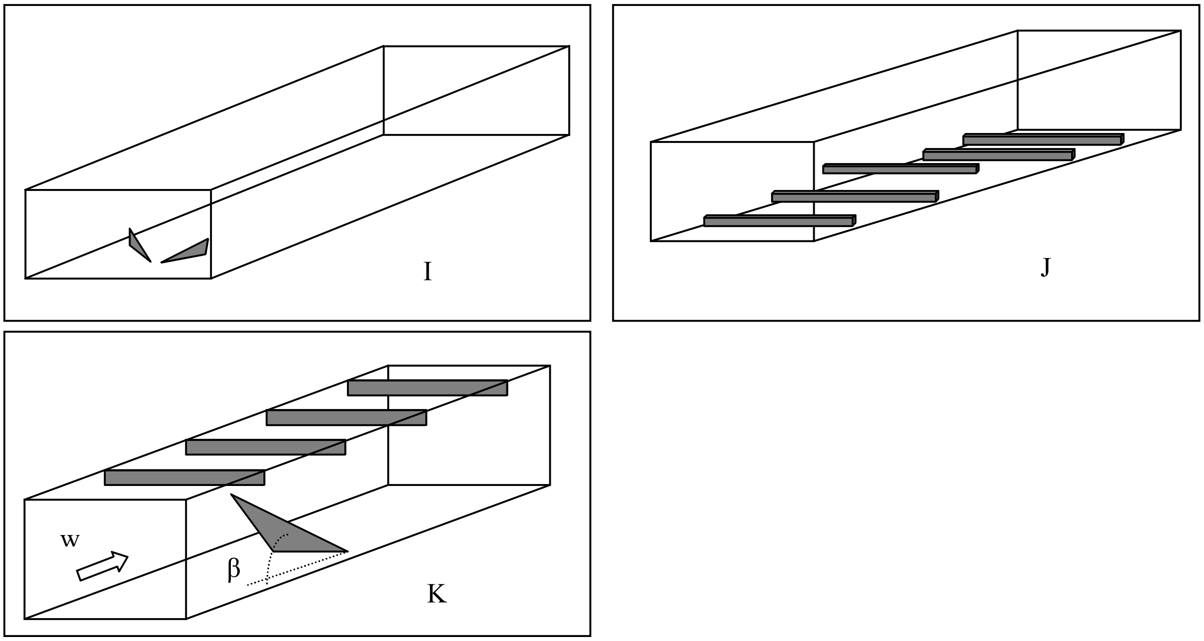

Fig. (1) Continue: I) Pair of winglets, J) Multi-ribs, and K) Wing & fins.

Table (1) Duct and VGs configuration.

<table>
<tr><th rowspan="3">Case</th><th rowspan="3">VG Type</th><th colspan="9">Configurations</th><th rowspan="3">Grid size</th><th colspan="2">Re</th></tr>
<tr><th colspan="3">Duct</th><th colspan="6">VG</th><th rowspan="2">Laminar</th><th rowspan="2">Turbulent</th></tr>
<tr><th>B (m)</th><th>H (m)</th><th>L (m)</th><th>b (mm)</th><th>h (mm)</th><th>l (mm)</th><th>β (°)</th><th>α (°)</th></tr>
<tr><td>A</td><td>Staggered fins</td><td>0.32</td><td>0.16</td><td>0.8</td><td>48</td><td>24</td><td>---</td><td>90</td><td>90</td><td>21*21*31</td><td>1,500</td><td>100,000</td></tr>
<tr><td>B</td><td>Vertical rib</td><td>0.16</td><td>0.08</td><td>0.6</td><td>32</td><td>80</td><td>16</td><td>90</td><td>90</td><td>11*19*40</td><td>750</td><td>7,500</td></tr>
<tr><td>C</td><td>Horizontal fin</td><td>0.16</td><td>0.08</td><td>0.6</td><td>160</td><td>5</td><td>---</td><td>90</td><td>90</td><td>20*19*40</td><td>2,119</td><td>21,191</td></tr>
<tr><td rowspan="4">D</td><td rowspan="4">Horizontal and vertical ribs</td><td rowspan="4">0.4</td><td rowspan="4">0.2</td><td rowspan="4">1.68</td><td colspan="5">Horizontal</td><td rowspan="4">21*21*31</td><td rowspan="4">500</td><td rowspan="4">5,000</td></tr>
<tr><td>400</td><td>20</td><td>57</td><td>90</td><td>90</td></tr>
<tr><td colspan="5">Vertical</td></tr>
<tr><td>40</td><td>200</td><td>57</td><td>90</td><td>90</td></tr>
<tr><td>E</td><td>Staggered 2-fins</td><td>0.16</td><td>0.08</td><td>0.6</td><td>32</td><td>80</td><td>---</td><td>90</td><td>90</td><td>11*19*40</td><td>750</td><td>7,502</td></tr>
<tr><td>F</td><td>Oblique rib</td><td>0.32</td><td>0.16</td><td>0.8</td><td>320</td><td>20</td><td>54</td><td>90</td><td>55.4</td><td>9*18*31</td><td>1,500</td><td>12,800</td></tr>
<tr><td>G</td><td>Broken ribs</td><td>0.32</td><td>0.16</td><td>0.8</td><td>50</td><td>16</td><td>27</td><td>90</td><td>90</td><td>21*21*31</td><td>2,000</td><td>10,000</td></tr>
<tr><td>H</td><td>Delta winglet</td><td>0.12</td><td>0.055</td><td>0.7</td><td>10</td><td>15</td><td>46</td><td>90</td><td>12</td><td>25*12*70</td><td>1,700</td><td>12,571</td></tr>
<tr><td rowspan="2">I</td><td rowspan="2">2-Delta winglet</td><td rowspan="2">0.12</td><td rowspan="2">0.055</td><td rowspan="2">0.7</td><td rowspan="2">10</td><td rowspan="2">15</td><td rowspan="2">46</td><td rowspan="2">90</td><td>12</td><td rowspan="2">25*12*70</td><td rowspan="2">1,700</td><td rowspan="2">17,000</td></tr>
<tr><td>-12</td></tr>
<tr><td rowspan="4">J</td><td rowspan="4">5-Continuous horizontal ribs</td><td rowspan="4">0.16</td><td rowspan="4">0.08</td><td rowspan="4">0.6</td><td colspan="3">4-at bottom wall</td><td rowspan="4">90</td><td rowspan="4">90</td><td rowspan="4">11*19*50</td><td rowspan="4">750</td><td rowspan="4">14,222</td></tr>
<tr><td>160</td><td>13</td><td>12</td></tr>
<tr><td colspan="3">Last one</td></tr>
<tr><td>160</td><td>4</td><td>12</td></tr>
<tr><td rowspan="4">K</td><td rowspan="4">Delta wing with horizontal 4-fins</td><td rowspan="4">0.4</td><td rowspan="4">0.2</td><td rowspan="4">1.68</td><td colspan="5">Delta wing</td><td rowspan="4">26*15*60</td><td rowspan="4">1,000</td><td rowspan="4">5,000</td></tr>
<tr><td>144</td><td>157</td><td>316</td><td>26</td><td>90</td></tr>
<tr><td colspan="5">4-fins</td></tr>
<tr><td>400</td><td>14</td><td>---</td><td>90</td><td>90</td></tr>
</table>

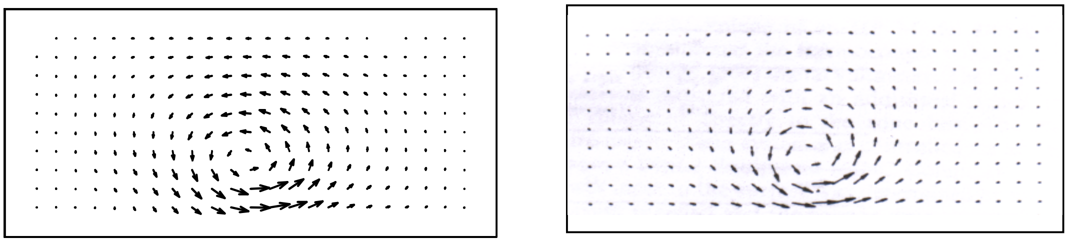

(a) (b)

Fig. (2) Secondary flow velocity vectors at z = 0.6 m (a) Present result (b) Data of [13].

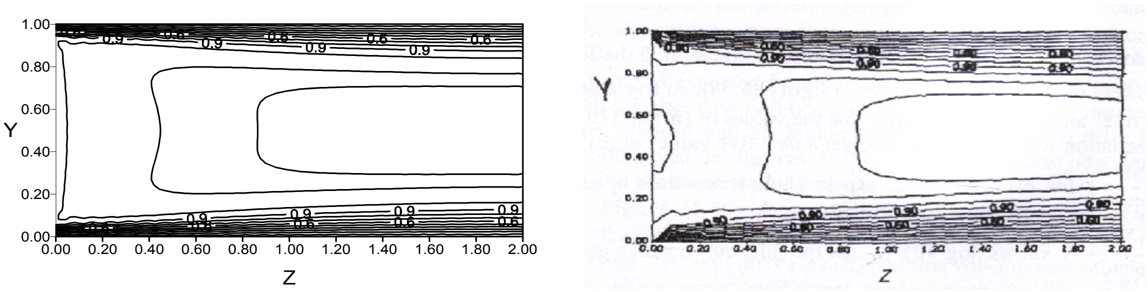

(a) (b)

Fig. (3) Variation of (w/w_{in}) at mid plane and Re=100: (a) Present result (b) Result of [17].

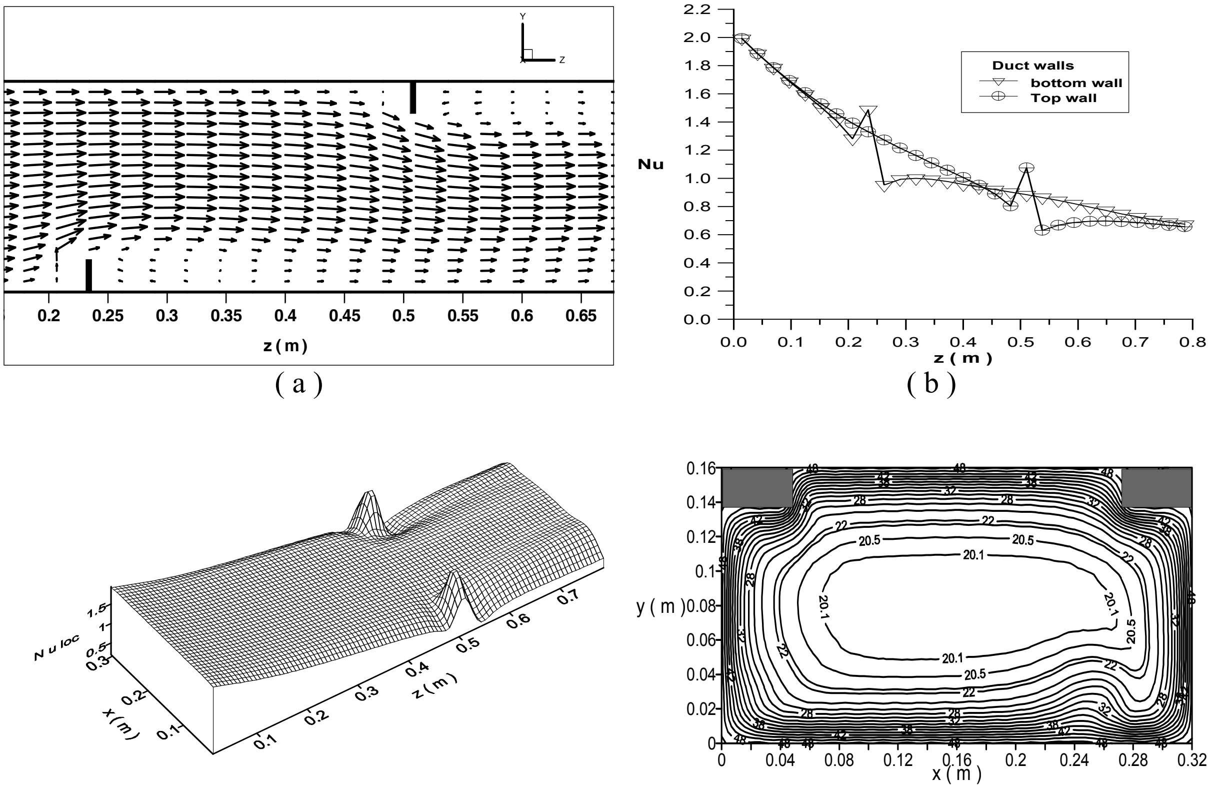

(a) (b)

(c) (d)

Fig.(4) Variation of flow field and isothermal contour and Nu for finned duct. Re=1,500: (a) Velocity vectors, (b) Average Nu, (c) Local Nu at upper wall, (d) Temperature contours.

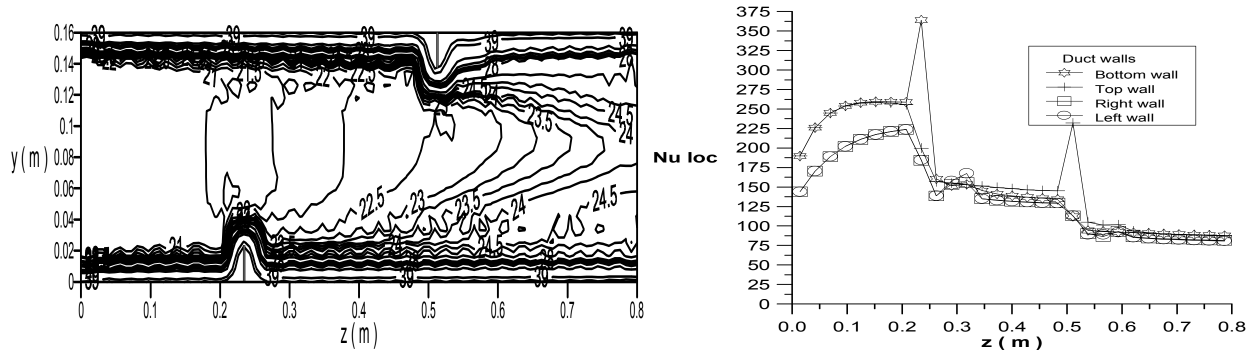

(e) (f)

Fig.(4) Continue , Re=100,000: (e) Isothermal contours, and (f) Average Nu.

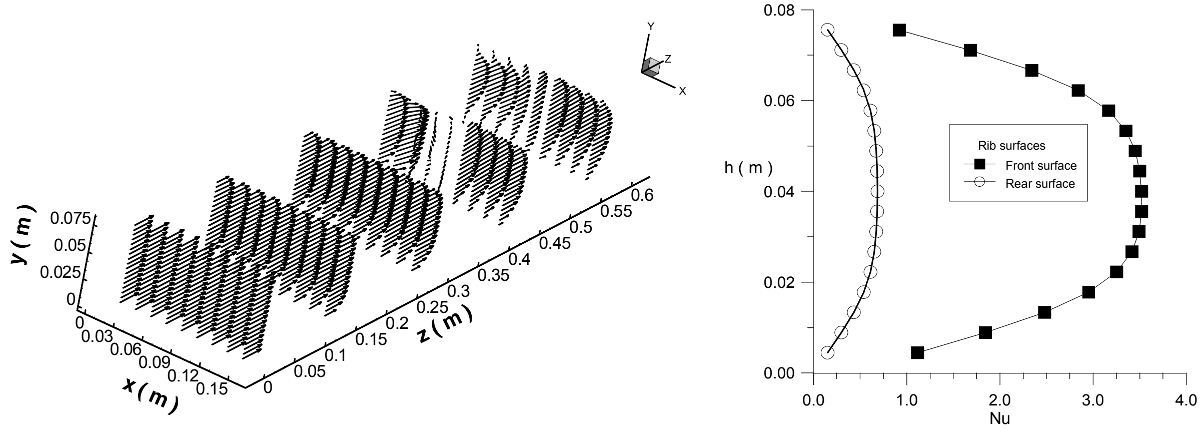

(a) (b)

Fig. (5) Velocity vectors and Nu for vertical ribbed duct. Re=750: (a) Velocity vectors in five selected planes, and (b) Average Nu on rib's two surfaces.

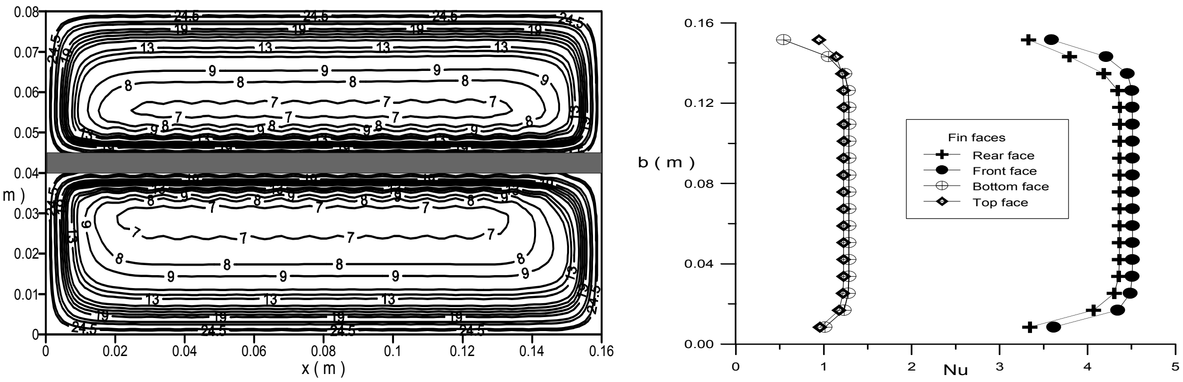

(a) (b)

Fig. (6) Temperature contours and Nu for case C. Re=2,119: (a) Temperature distributions, and (b) Average Nu.

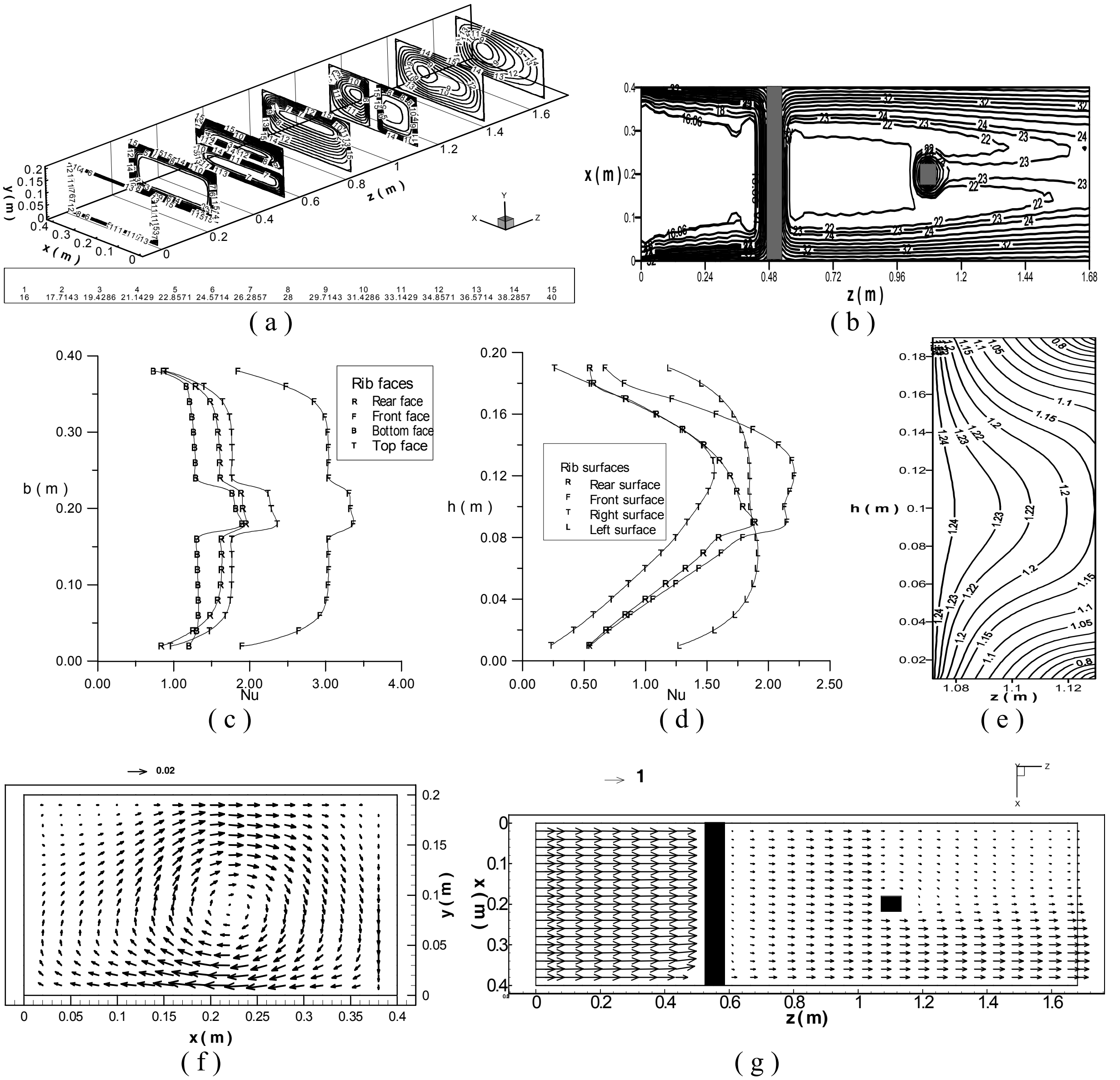

(a) (b)

(c) (d) (e)

(f) (g)

Fig. (7) Temperature contours, Nu, and velocity vectors for case D. Re=500: (a) Temperature distributions, (b) Temperatures at (x-z) plane, (c) Average Nu for horizontal rib, (d) Average Nu for vertical rib, (e) Local Nu for vertical rib, Re=5,000: (f) Velocity vectors in (x-y) plane, (g) Velocity vectors in (x-z) plane.

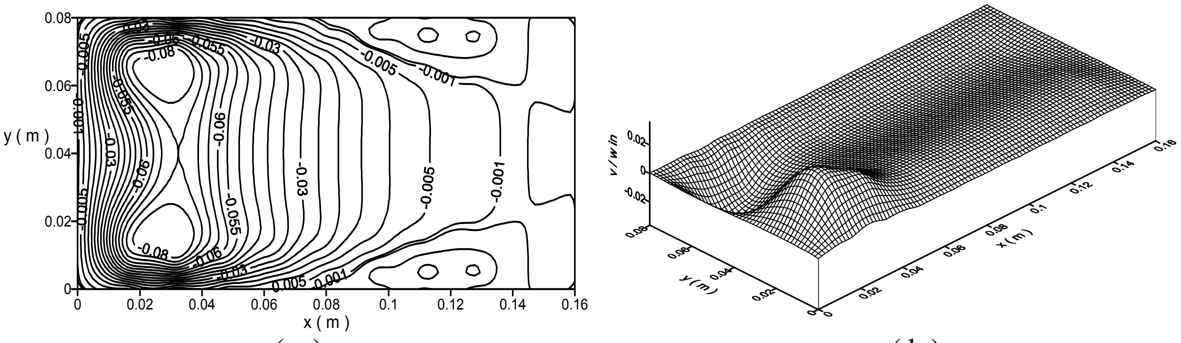

(a) (b)

Fig. (8) Velocities distributions for case E. Re=750: (a) u/w_{in} , (b) v/w_{in} .

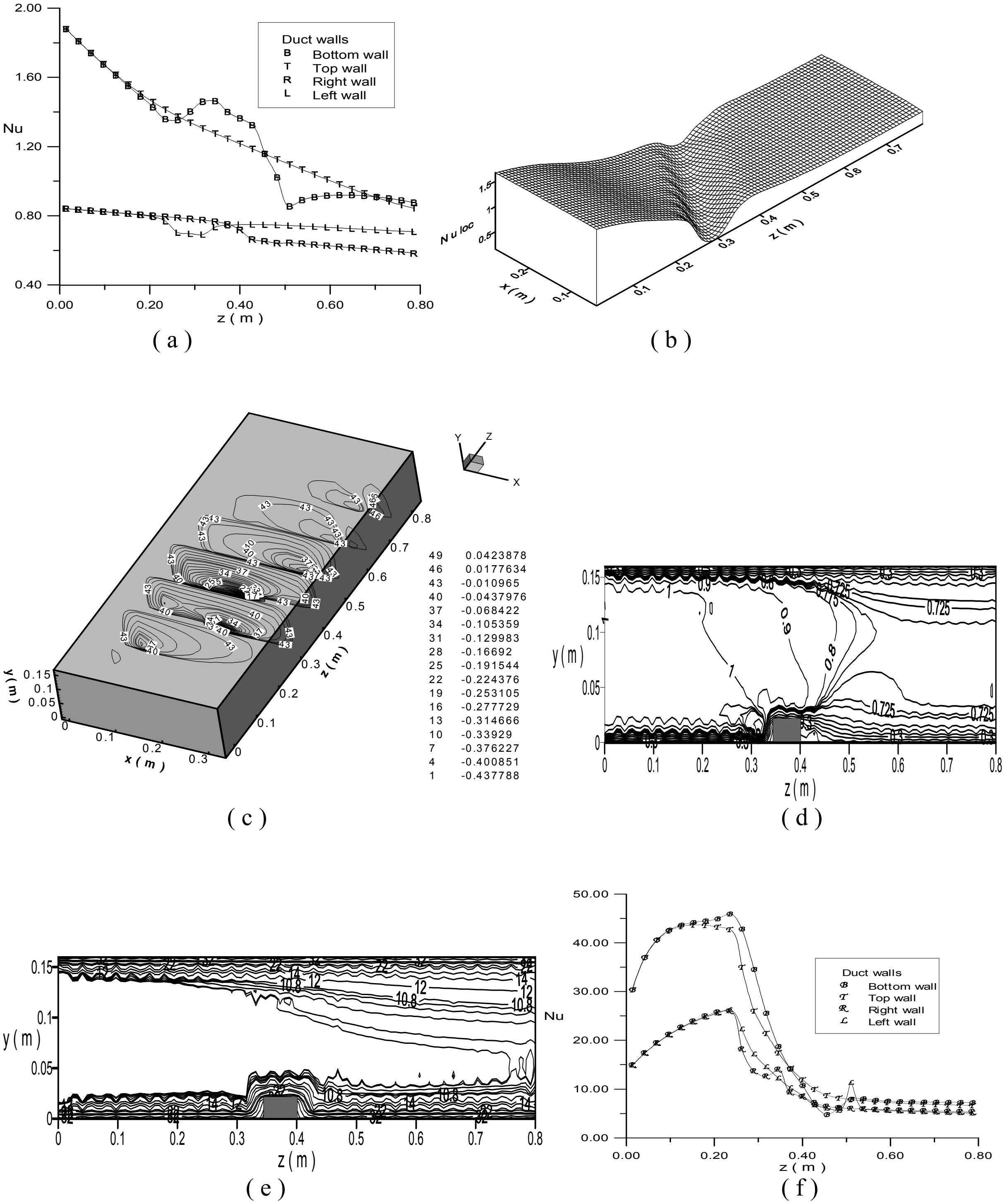

(a) (b)

(c) (d)

(e) (f)

Fig. (9) Nu variations, velocity vectors and temperature contours, for case F. Re=1,500: (a) Average Nu, (b) Local Nu at bottom wall, Re=12,800: (c) v contours, (d) w/w$_{in}$ distribution, (e) Isotherms, (f) Average Nu for turbulent case.

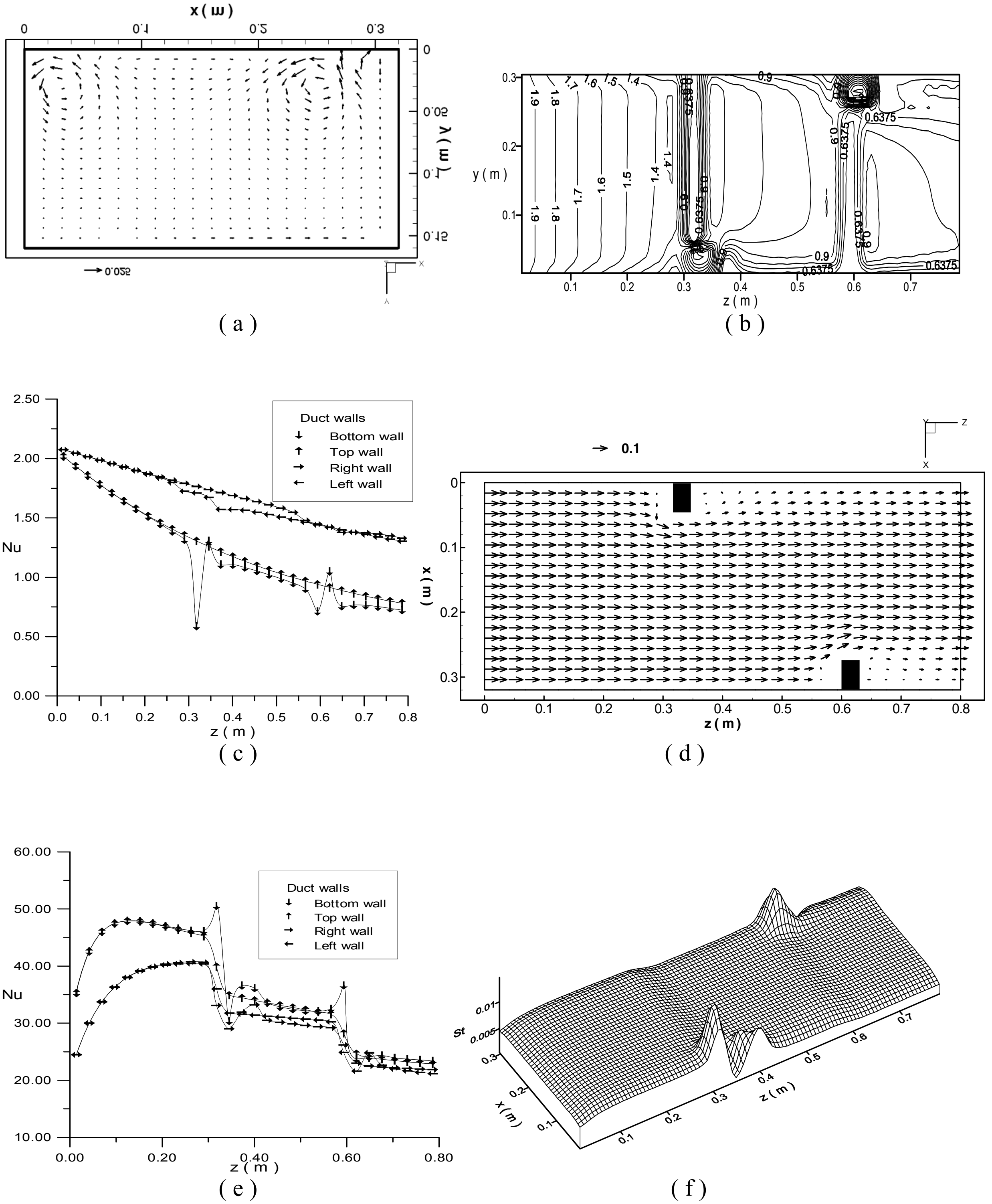

(a) (b)

(c) (d)

(e) (f)

Fig. (10) Nu variations and velocity vectors for case G. For laminar flow Re=2,000: (a) Velocity vectors, (b) Local Nu, (c) Average Nu, and for turbulent flow Re=10,000: (d) Velocity vectors, (e) Local Nu, (f) Local Stanton number.

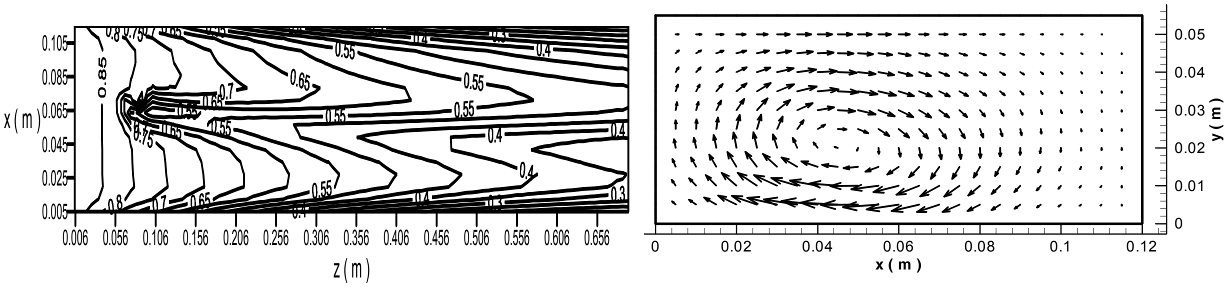

(a) (b)

Fig. (11) Nu variations and velocity vectors for cases H & I. Re=1,700: (a) Local Nu, Re=17,000: (b) Velocity vectors.

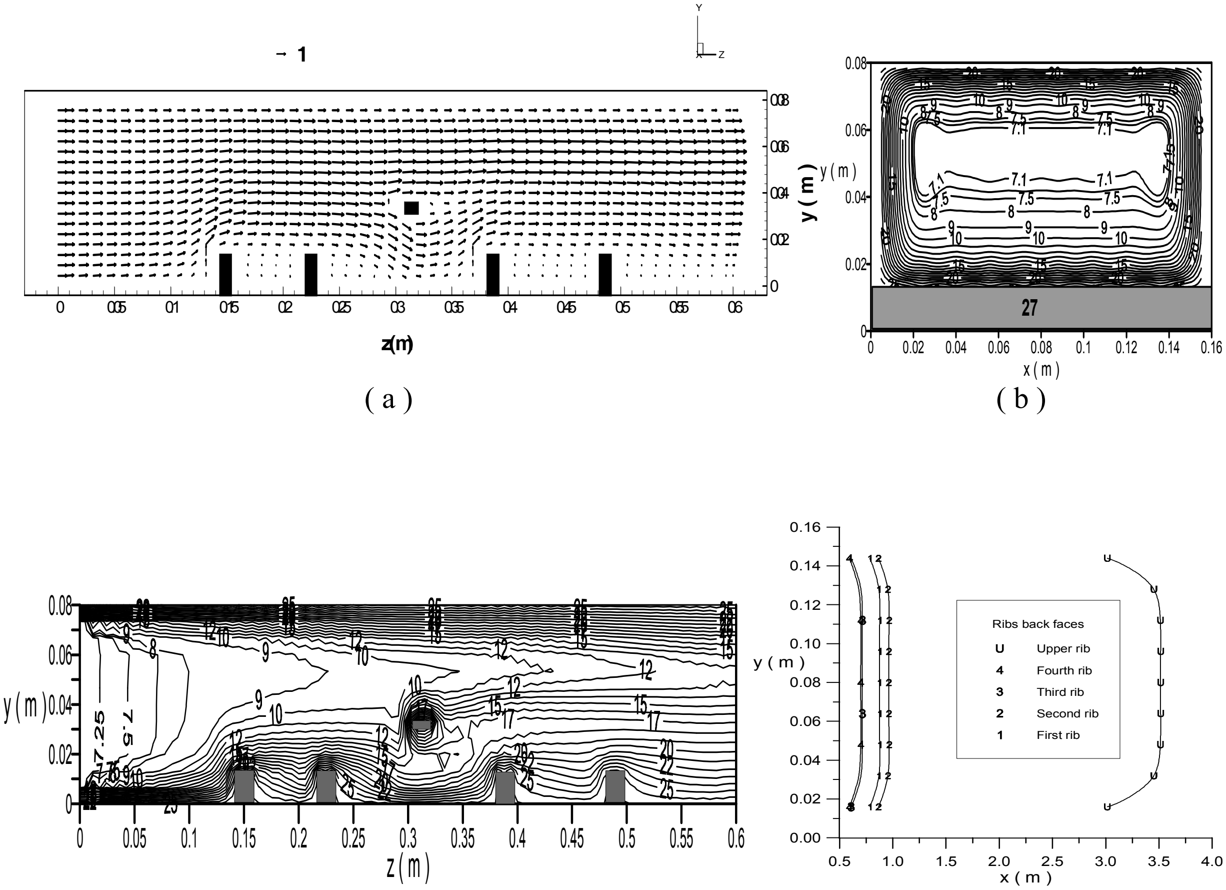

(a) (b)

(c) (d)

Fig. (12) Velocity distributions, temperature contours, Nu, and St numbers for case J. For laminar flow Re=750: (a) Velocity vectors, (b) Temperature contours, (c) Isotherms, (d) Average Nu.

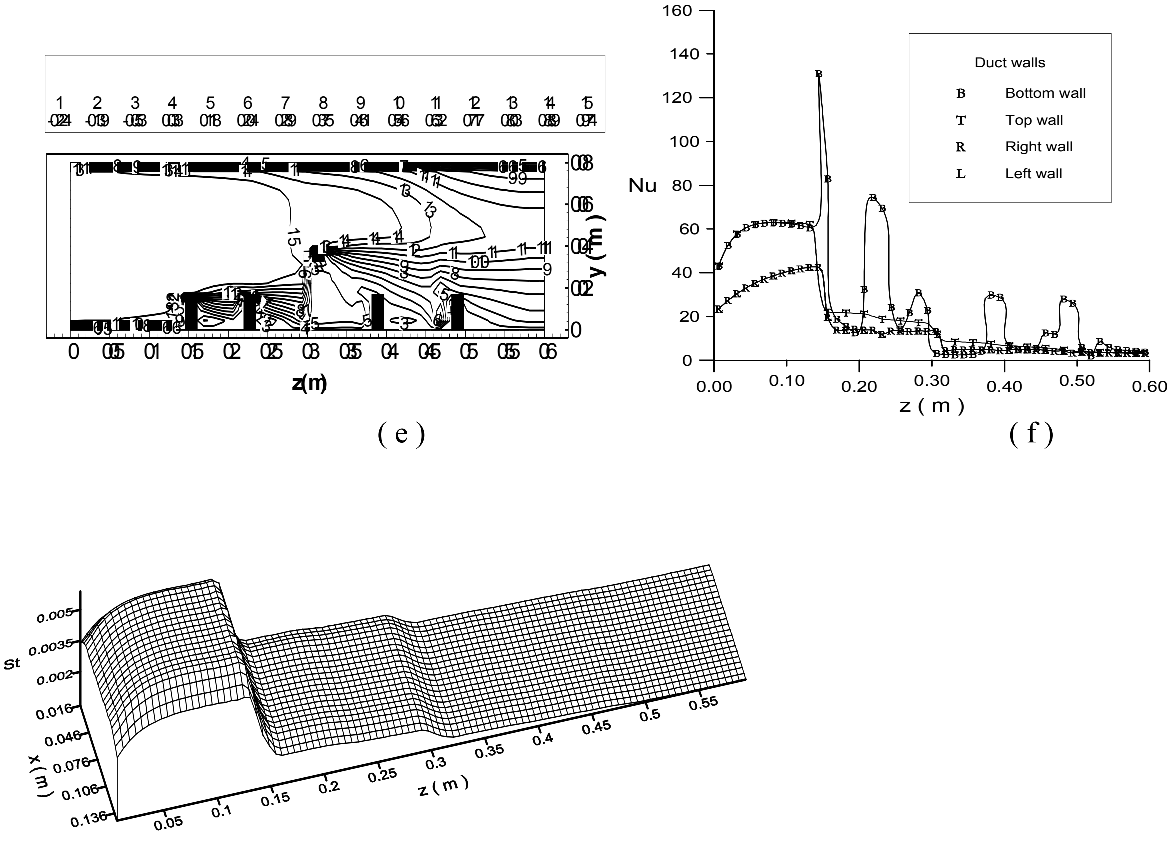

(e) (f)

(g)

Fig. (12) Continue, for turbulent flow Re=14,222: (e) Velocity (w) vectors, (f) Average Nu, (g) Local St.

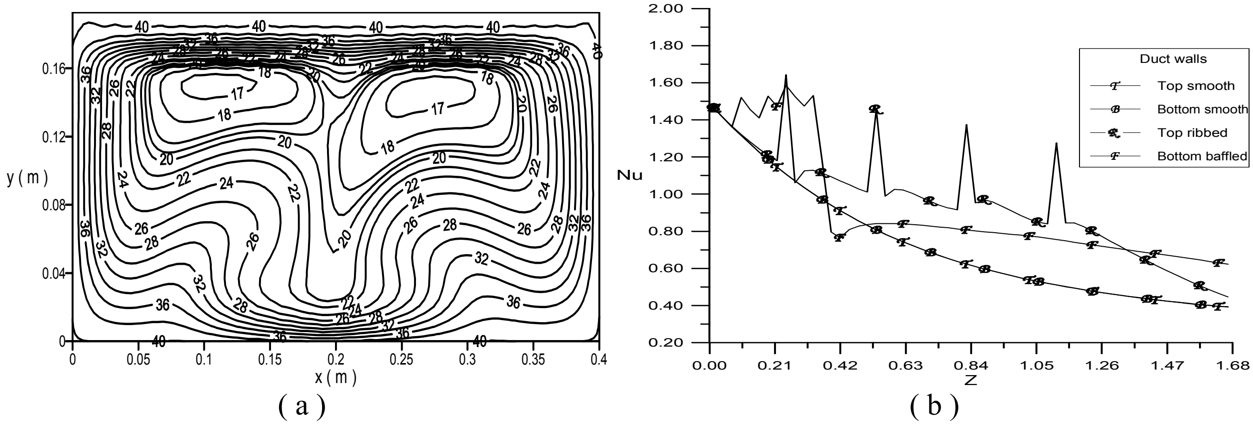

(a) (b)

Fig. (13) Velocity vectors, temperature contours, Nu, and St numbers for case K. For laminar flow Re=1,000: (a) Temperature contours, (b) Average Nu.

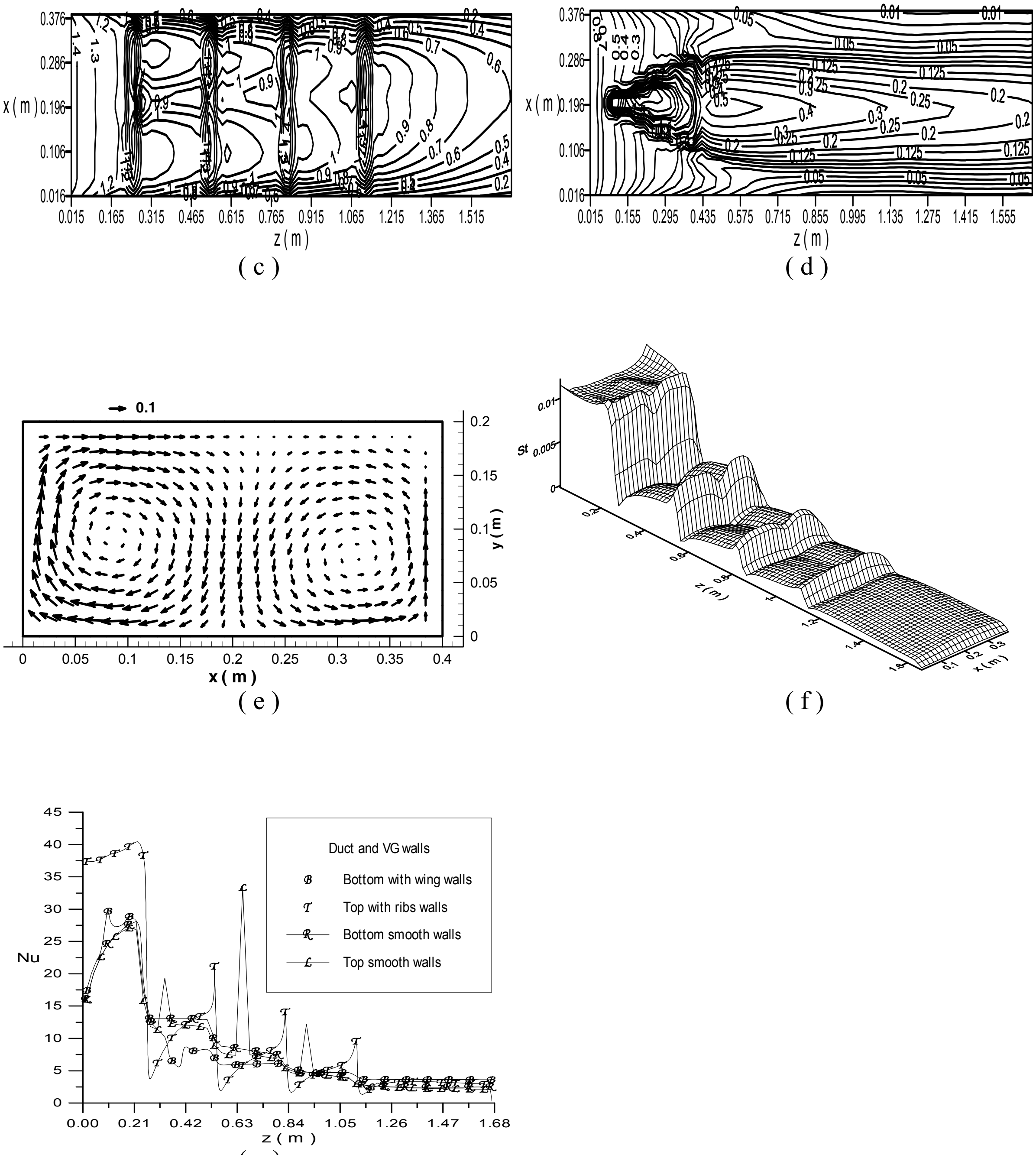

(c) (d)

(e) (f)

(g)

Fig. (13) Continue, (c) Local Nu for top wall with ribs, (d) Local Nu for bottom wall with wing, For turbulent flow Re=5,000: (e) Velocity vectors, (f) Local St for bottom wall with VG, (g) Average Nu with VG.

NOMENCLATURE

a_E , a_w	Coefficients in general finite-domain equation
A_{cell}	Wall area of the control volume
b	Width of the VG (wing span)
B	Width of the duct
$C_{1\varepsilon}$,$C_{2\varepsilon}$,C_μ	Coefficient in turbulence models, =1.43, 1.92, 0.09 respectively
C_p	Specific heat
D_e , D_w	Diffusion terms
E	Logarithmic wall constant
F_e , F_w	Convection coefficients
F_s	Wall force
G	Generation rate of turbulence energy
h	VG height
H	Duct height
hd	Hydraulic diameter
k	Turbulent kinetic energy
K	Thermal conductivity of the fluid
l	VG length or thickness or chord
L	Duct length
Nu	Nusselt number
p	Pressure
Pe	Finite-domain cell Peclet number
Pr	Prandtl number
St	Stanton number
Re	Reynolds number
T	Temperature
Tb	Bulk temperature
T_{ref}	Field reference temperature
U,V,W	Mean velocity components
x,y,z	Coordinate directions

Greek Symbol

α	Inclination angle in (x-z) plane
β	Angle of attack in (y-z) plane
Γ	Diffusion coefficient
ε	Rate of dissipation of k
κ	Von Karman's constant
μ	Dynamic viscosity
υ	Kinematics viscosity
ρ	Fluid density
σ	Prandtl number
τ_{wall}	Wall shear stress

Subscript

eff	Effective value
e , w	Control volume faces
in	Condition at inlet
k , ε	Refer to turbulence model equation
l	Laminar flow condition
n	Normal distance from a wall
N	Duct dimensions = B , H , L
P , E , W	Central node and its neighbors (east and west)
t	Turbulent flow condition
wall	Condition at wall

Superscript

+	Dimensionless value

Abbreviation

ESCEAT	Elliptic equation Solver for Convection and Heat Transfer
k-ε	Two-equations turbulence model
SIMPLE	Simi-Implicit Method for Pressure Linked Equation
VG	Vortex Generator

References

1- Jeffrey Alan Taylor, " Development Of An ' Active Wing' For The Validation Of Active Flow Control Schemes To Be Applied To The Of Incipient Separation ", M.SC. Thesis, Mech.Eng. , Clarkson university, November 17 , 1998.

2- Alvaro Valencia " Turbulent Flow And Heat Transfer In A Channel With A Square Bar Detached From The Wall ", Numerical Heat Transfer Part A, 37, 2000, PP. 289-306.

3- Jamil A. Khan, Jason Hinton, and Sarah C.Boxter, "Enhancement Of Heat Transfer With Inclined Baffles And Ribs Combined ", Journal of Enhanced Heat Transfer, 9, 2002, PP.137-151.

4- Suh-Jeng Yang. "A Numerical Investigation Of Eeat Transfer Enhancement For Electronic Devices Using An Oscillating Vortex Generator ", Numerical Heat Transfer, Part A , 42 ,2002 , PP.26-284.

5- St. Tiggelbeck, N.K.mitra, and M.Fiebig "Comparison Of Wing Type Vertex Generators For Heat Transfer Enhancement In Channel Flows" Transaction of the ASME, Journal of Heat Transfer, November 1994,Vol.116.

6- İsak KOTCİO Ğlu , Troman AYHAN , Hayati OLGUN , and Betűl AYHAN " HEAT Transfer And Flow Structure In A Rectangular Channel With Wing-Type Vortex Generator ", Tr.J. of Engineering and Environmental Science ,22 (1998) ,PP. 185-195.

7- T.M.liou , C.-C. Chen , and T.W.Tsai "HEAT Transfer And Fluid Flow In A Square Duct With 12 Different Shaped Vortex Gene Rotors", Transaction of the ASME ,Journal of Heat Transfer ,may 2000,Vol.122,PP.327-335 .

8- Ahmed Sohankar and Lars Davidson, "Numerical Study Of Heat And Flow In A Plate-Fin Heat Exchanger With Vortex Generators", Turbulence, Heat and mass transfer 4, 2003,Begell, Inc., PP.1155-1162.

9- Y.H .Hung and H.H.Lin , An effective installation of turbulence promoters for heat transfer augmentation in a Vertical rib-heated channel ,"int. J. Heat Mass transfer ,vol.35,no.1,PP.29-42,1992.

10- J.C. HAN and Y.M.ZHANG."High Performance Heat Transfer Ducts With Parallel Broken And V-Shaped Broken Ribs" Int. J. Heat mass transfer Vpl.35.No.2, PP.513-253, 1992.

11- D.A.Aliaga D. E.klein ,and J.P.Lamb ," Heat Transfer Measurements On A Ribbed Surface At Constant Heat Flux Using Infrared Thermongraphy ", Experimental Heat Transfer ,Vol.6,PP.17-34,1993 .

12- R.W.DAVIS and E.F.MOORE, "A Numerical Study Of Vortex Shedding From Rectangles ", J, Fluid mech .(1982),vol.116,PP.475-506.

13- P.A. Eibeck and J.K. Eaton ," Heat Transfer Effects Of A Longitudinal Vortex Embedded In A Turbulent Boundary Layer", Transactions of the ASME , Journal of Heat Transfer , February 1987 ,vol.109 ,PP16-24 .

14-Hayder Mahdi Kadhum,"Numerical And Experimental Study Of Enhancement Of Heat Transfer In Roughened Ribbed Duct", January 2004, Ph.D. Thesis, Dept. of Technical Education, University of Technology.

15- Waheed. S. Mohammed," Space Air-Conditioning Of Mechanically Ventilated Rooms: Computation Of Flow And Heat Transfer ", June 1986,Ph.D.Thesis, school of mechanical Engineering, Cranfield Institute of Technology.

16- Patanker S.V.'Numerical Heat Transfer And Fluid Flow ", Me Graw-Hill Book Company New York, 1980.

17- Sabah Tarik Ahmed,"Numerical And Experimental Study On Heat Transfer Enhancement By Vortex Generator ", September 2001, Ph.D. Thesis, Dept. of mechanical Engineering, university of Technology.

‼!!!ƒ! ‼ !!Œ !œ!Œ !!! çœ! !Œ¾! !!!! Œš!Œ½œ!Œ ‼ !!!Œ!Œ Œ! !!! ŒŒ Œƒ!!

‼

‼! ƒš!! Ž!! ‼ ƒ!!! ‼!!šŒž !œ!! œ !!!!! ‼!!š! ‼ !œ!! ƒš! !!!!!!

‼! ‼Ÿ!‼ ‼ œ!‼! ‼!!! ! ‼! ‼Ÿ!‼ ‼ œ!‼! ‼!!! ! ‼! ‼Ÿ!‼ ‼ œ!‼! ‼!!! !

‼!!Š! ‼ ‼!‼!Ÿ!!Š‼ ‼!!Š! ‼ ‼!‼!Ÿ!!Š‼ ‼!!Š! ‼ ‼!‼!Ÿ!!Š‼

‼

‼!! ! ! !Œ

!¿! ! ‼ ‼! ! ! ! ‼ ‼ ‼! ‼! ‼! Š‼! ! ‼ ‼! ‼! Š‼¿! ! ‼! ‼ ! ‼¿!!!!! œ ! ‼ ‼ ! !!!!!! ! ‼!! ‼ !‼!!! ‼ ž !
‼! ! ! !!! ! ‼!‼! ‼ ‼!‼! ‼ ‼100,000!! ‼500!! ‼! ‼! ‼! ‼! ‼! ! ‼ ‼ ‼ ‼!‼ ! ‼!‼ ‼ ‼! ‼!! ƒ ! ! ‼¿‼ ‼ ‼! ! Š!
‼! ‼! ! ‼!!‼ ‼! ‼!‼!!! ‼ ! ‼! ‼! ! ‼!! ! ! ‼! ! ‼! ‼!!‼ ‼! ! ‼ ! ! ‼! ‼!Ÿ! ! ¿! ‼ !(ESCEAT)! ! ‼! ‼! !
‼! ‼ ! ‼¿‼!‼ ! ‼ ‼! ‼! ‼! ! ‼ ‼! ‼ ! ‼ ‼ ! ! ‼! œŸ‼! ! ‼! ! ‼! ¿‼! ! ‼ ‼! Š‼¿! ! ! ! ‼ ‼!‼ ‼! ‼ ! ‼! Š! !
‼ ‼! ‼ ! ‼! ! ! ! ‼!‼!! ‼ ‼!‼ ‼! ‼ ! ‼! !Š! ‼! ‼ ‼!‼ ! ‼!‼!‼ ‼ ! ! ‼! ‼! ! ! ‼ ! ‼! ¿! ! ! ! ‼! ‼ Š‼¿! ! !
‼ ‼! ‼! ‼! ‼ ‼!‼! ‼ ‼ ! ‼ Š! ‼! ‼!¿! ‼! ‼!‼ ! ‼ ‼!‼ ! ‼ ‼ ‼! ‼ ! ‼! !Š! ‼! ! !Š! ! ! œ‼! ‼! Š! !Ÿ! ‼ ‼¿‼! ! !
‼ ! Š! ‼! ! ‼! ! ! ! ! ‼ ‼ ! ‼ ‼ ‼! ! ‼! Ÿ‼ ¿‼! ! ‼ ‼!‼ ‼!‼! ‼ ! ‼ ! ‼! ! ‼ ‼! ! ! ‼ ‼ ‼! ! ‼! Ÿ‼ ! ‼Ÿ‼ ! ¿! ! ‼ ! œŸ‼
!Ž ! ! ‼ œŸ‼! ‼! ‼!‼! ‼! ‼! ! ! ‼Ž ! ! ‼ ‼ ‼!‼ ‼ !ž! ‼ ! ‼!‼! !¿! ! ‼! ! ! ‼! ‼! ‼ ‼! ‼! ‼! ‼! ‼! ‼!‼ ! ! !‼
‼!! ‼ ‼! ‼! ž! ! ‼ ‼!‼ ! ! ‼! ! ! ‼! ‼ ! ! ! œŸ‼¿! ! ‼ ‼ ‼! ‼ ! ‼¿!!!!! ! ! ‼

‼

‼!‼ ‼ !‼!ƒ ! !Š! ‼!‼ œ! ‼! ‼! Š! ‼! ‼ ! ‼¿!!!!!CFD!! ‼ ‼! ‼ ‼! ! ‼! œž! !Œ œ!

‼